High-energy ion beam irradiation of Co/NiFe/Co/Cu multilayers: effects on the structural, transport and magnetic properties

P. L. Grande, L. C. C. M. Nagamine, J. Morais

Instituto de Física, UFRGS, Av. Bento Gonçalves, 9500, 91501-970, Porto Alegre, Brazil

M.C.M. Alves

Instituto de Química, UFRGS, Av. Bento Gonçalves, 9500, 91501-970, Porto Alegre, Brazil

G. Schiwietz, M. Roth, B. Schattat

Hahn-Meitner Institut, Abteilung, SF4 Glienicker Strasse 100, D-14109 Berlin, Germany

E. Baggio-Saitovitch

Centro Brasileiro de Pesquisas Físicas, R. Dr. Xavier Sigaud 150, Rio de Janeiro, Brazil

Abstract

The aim of this work is to investigate the effects of 593 MeV Au irradiation using two different projectile charges, namely Au^{30+} and $Au^{46.3+}$ on the structural, transport and magnetization properties of Co/NiFe/Co/Cu multilayers. X-Ray diffraction and extended x-ray absorption fine structures measurements show no significant structural change for as deposited and irradiated multilayers. On the other hand, the magnetoresistance amplitude decreases with the ion fluence but it is insensitive to the projectile charge state. The correlation between changes in the magnetoresistance and remanent magnetization suggests that the main effect responsible for the decrease of the magnetoresistance is the creation of ferromagnetic pinholes. These results are discussed on basis of the electronic thermal spike model and nuclear cascades theory and show similarities to the effects observed at low-energy ion-beam irradiation.

61.80.Jh, 75.70.Pa

I - Introduction

Fast heavy ions may lead to permanent material changes in a small cylinder along the nearly straight ion path, giving rise to the so-called ion tracks. Different explanations for the basic mechanisms for the track production have been proposed [1-9], but all of them depend on the electronic ionization along the ion path and thus on the projectile charge. All these mechanisms may finally yield an unordered atomic motion and if a critical local lattice temperature is exceeded, permanent atomic rearrangement may result. The influence of the nuclear tracks has been widely studied in polymers, semiconductors and metallic glasses [10-11], but in much less extension for magnetic materials.

Multilayer (ML) magnetic systems have been widely investigated since the discovery of the phenomenon of giant magnetoresistance (GMR) [12], because of their great potential for applications in magnetic recording technology [13]. In particular studies using low energy ions, where nuclear stopping power predominates, show that the ion bombardment can promote local atomic diffusion and modification of the magnetic properties of the target. For instance changes in the coercivity , uniaxial magnetic texture, interface mixing and phase transformation have been reported for Fe/Co systems [14-17]. Furthermore the suppression of exchange bias [18] and modification of the perpendicular interface anisotropy [19] have been observed by keV He ions irradiation. Also these low energy ions may be used to control of interlayer exchange coupling [20] and to induce chemical order in intermetallic alloys [21]. Swift ion irradiations with 350 MeV Au ions also lead to changes in magnetism and microstructure as recently observed in Fe/Si systems [22,23].

The ion irradiation at low energies may increase the GMR in few cases (depending on the ion fluence) but mostly it leads to a degradation of the GMR [24-27]. The observed reduction of the GMR and the partial loss of antiferromagnetic coupling were interpreted in terms of the creation of ferromagnetic pinholes. Some few investigations using high-energy ions such as 200 MeV Ag-ion irradiations [28-30] also show a decrease of the GMR in Fe/Cr MLs.

Sputtered Co/NiFe/Co/Cu MLs are of particular interest due their large GMR at room temperature [31-32] and they are sensitive to the ion irradiation [32a-34b]. For the Permalloy the influence of ion implantation and irradiation has been investigated at low as well as at high projectile energies. Experiments of high-energy heavy ions show a large shift of the Curie temperature due to a negative pressure effect introduced by the irradiation [32a,32b,32c]. On the other hand, a for lower projectile energies, NiFe has been implanted with Cr ions [33] to reduce the Curie temperature and irradiated with 200 keV Ar ions to alter the local anisotropy direction allowing for anisotropy nanopatterning [34].

For the pure metals components, the high electronic energy deposition due to high-energy heavy ions leads to creation of additional defects as well as phase transformation [34a,34b].

In this work we have used high-energy Au ions at 593 MeV to irradiate Co/NiFe/Co/Cu MLs. These ions deposit a huge quantity of energy in the form of electronic excitations of the atoms inside the sample. The specific electronic energy loss of about 60 keV /nm exceeds the energy given to the ballistic motion (nuclear energy loss) by a factor of 300 and is much larger than the one used in previous measurements [28-30]. Moreover we have used two projectile charge-states, namely the non-equilibrium charge state Au^{30+} from the cyclotron and $Au^{46.3+}$ after charge equilibration in a thin carbon foil, which have different electronic stopping powers, to probe the magnetic properties of Co/NiFe/Co/Cu MLs for two excitation conditions.

We have studied the effects of the Au irradiation (with small fluence < 10^{14} Au/cm^2 and two projectile charges) on the electron transport (using GMR measurements), on the structural (using x-ray diffraction XRD and absoption EXAFS) and on magnetic properties (investigating the hysteresis curves). In Sec. II we describe the experimental procedure to prepare the Co/NiFe/Co/Cu MLs as well as the conditions for the ion irradiation. Then, in Sec. III, we shall give the results of the different characterization techniques and finally in Sec. IV the results will be discussed in connection with high-energy irradiation models.

II - Experimental Procedure

In the present work, Co/NiFe/Co/Cu MLs (here, $Ni_{81}Fe_{19}$) were deposited by DC magnetron sputtering onto a Si(100) substrate with native SiO_2 in 0.3 Pa Ar atmosphere with base pressure better than 5×10^{-8} Pa before the deposition. The films consist of $[Co\ 5Å\ /NiFe\ 15Å/\ Co\ 5Å/\ Cu\ 9Å]_{20}$ deposited on NiFe 54Å/Co 5Å/Cu 9Å and also capped with Co 5Å/ NiFe 15Å layers. The Cu, Co and NiFe were sputtered at a rate of 8.6, 7.7 and 8.2 nm/min, respectively obtained by the analysis of the x-ray reflectivity. In order to achieve homogeneous samples, only two Si substrates could be put side by side before each deposition. However, we repeated several times the same procedure, maintaining the same type of deposition, in order to prepare MLs with approximately the same nominal thickness. Then, these MLs were checked by the analysis of the x-ray reflectivity and magneto resistance (MR) measurements. The samples with about the same MR amplitudes were select for the irradiations.

The specimens were irradiated at room temperature with 593 MeV[a] Au^{30+} and $Au^{46.3+}$ ions at ion fluences of 3×10^{13} Au/cm^2 and 6×10^{13} Au/cm^2 provided by the ECR-RFQ-cyclotron accelerator facility of the Ionenstrahl-Labor (ISL) at the Hahn-Meitner-Institut Berlin. The beam incidence was 45 degrees and covered the sample homogeneously by means of a x-y-sweeping system. In order to minimize the overheating of the samples, they were fixed using carbon glue with high thermal conductivity. In this way, the target temperature during the irradiations has been kept below 80 ^{o}C.

The Au^{30+} beam was provided directly by the cyclotron. A stripper foil made of 100 μg/cm^2 amorphous carbon about 0.5 m in front of irradiation chamber provided a quasi-equilibrium charge-state distribution peaked at $Au^{46.3+}$. Fig. 1 shows the mean exit charge state for varying carbon-foil thickness measured by magnetic beam deflection using the post-cyclotron stripper stage. Comparison is made with the charge-state fits by Nikolaev and Dmitriev [35] as well as Grande and Schiwietz [36-37] accounting for the influence of the ion-energy loss [38] on the exit charge state. The original charge-state distributions correspond to widths of ±3 to ±4 charge units. The ions are implanted into a depth of about 16 μm below the surface [38], which may be compared to the ML

---

[a]

thickness of 68 nm. We estimate from Fig. 1 and from the charge-state fit that the mean effective charge-state is about 45+ for the incident $Au^{46.3+}$ ions and about 38+ for the incident (primary) Au^{30+} ions when we perform a squared average of the charge equilibration over the ML thickness. Thus, there should be a 40% energy-loss deviation between the two beams when averaged over a depth of 68 nm.

The highly charged ions and the large incidence angle have been selected in order to increase the sensitivity of the ion irradiation. Afterwards, the samples were analyzed by measuring x-ray diffraction (XRD), extended x-ray absorption fine structure (EXAFS), magnetization and magneto resistance (MR) at room temperature. All these techniques are sensitive to all 20 magnetic MLs and effects of the substrate are expected to be of minor importance in what follows.

A Philips X'Pert θ-2θ diffractometer employing Cu Kα radiations was used to obtain the large-angle diffraction and the small-angle x-ray reflectivity scans.

The x-ray absorption measurements at the cobalt and copper K edges were performed at the Laboratório Nacional de Luz Síncrotron – LNLS, using the XAFS1 beam line [39]. A "channel cut" Si (111) crystal monochromatized the collimated X-ray beam with 1mm vertical slits placed before the monochromator corresponding to a resolution of $E/\Delta E$=7000. The monochromator was calibrated at the K edges using cobalt and copper standards. The samples were measured using the so-called total yield technique with the incident beam at 45^o with respect to the substrate surface.

EXAFS spectra were recorded for incident photon energies from 7600 to 8220 eV at the Co K edge and from 8880 to 9700 eV at the Cu K edge. An energy step of 2.0 eV and acquisition time of 2 s/point was used. An average of three acquisitions was performed to obtain good signal-to-noise ratio.

The EXAFS spectra were analyzed using the IFEFFIT analysis package [40]. The analysis was performed using the following general procedure: removal of the isolated atom background function from the experimental X-ray absorption coefficient data, then a Fourier transform (FT) in the range 2.2 and 11.8 $Å^{-1}$ was applied using a Hanning window. Structural parameters were obtained from a least-squares fit to the data in r-space using phase shift and amplitudes obtained from the FEFF code [41] calculated for Co and Cu metals in an fcc packing. The ATOMS program [42] was used to prepare the structural input for FEFF. Fits determined the distance variation with respect to the bulk material (ΔR), the Debye Waller factor (σ), the energy shift (E_0) and the passive electron reduction factor (S_0^2).

MR at room temperature was measured using the standard four-probe technique with a constant current source (~1mA) and a nanovoltmeter. The external field up to 1 T was applied in plane of the film and orthogonal to the current. The in-plane field-dependent magnetization was measured with an alternating gradient force magnetometer.

III - Results

III.1 - X-ray diffraction

The large-angle diffraction scans are shown in Fig. 2 for as deposited and irradiated ML. A (111) texture peak is observed at $2\theta=43.98 \pm 0.03$, which lies between the Cu ($2\theta=43.30$ and fcc Co ($2\theta=44.21^{o}$) and is similar to NiFe (in fact it may vary from $2\theta=43.47^{o}$, 39 at. %Ni [JCPDS, N° 23-0297] to 44.507º, Ni 100%). Using a Scherrer formula, we estimate a grain size normal to the surface of about 185 Å. After the irradiation, the linewidth of the (111) Bragg peak is nearly unchanged so that no sign of significant grain size modification is observed. The decrease of the relative intensity of the (111) peak after irradiation indicates a slight change in the film texture [43].

Figure 3 shows the reflectivity pattern of the MLs irradiated with different Au fluences and charge states (see caption). Two Bragg structures (a minimum and a maximum) associated to the ML periodicity are visible (see the arrows in Fig. 3) for as deposited and irradiated MLs, confirming that the multilayer structure is intact. As the atomic scattering factors of NiFe, Cu and Co are very close, it is hard to fit the reflectivity data to get reliable information since many solutions can be found. However, the height of second Bragg peak (see Table 1) of about 114, which is related to the average interface roughness [44] (i.e. lower height means higher interface roughness) decreases to values of about 80 and 53 with increasing ion fluence (see Fig. 3 (b) and Fig. 3 (d) respectively) and decreases furthermore from 53 to 8 with increasing projectile charge-state (see Fig. 3 (d) and Fig. 3 (e) respectively) for the largest fluence. The same happens for the smallest fluence. Therefore, these results may indicate a slight mixing dependent on the ion fluence and on the projectile-charge state. Nevertheless, this intensity reduction may be also attributed to other effects such as either a change of the texture as observed recently in ref[44a] using 350 MeV Au ions in Ti and TiN nanocrystals, or angular effects due to the change of the curvature radius of the irradiated Si substrate [44b]. It is clear, however, that such a strong projectile charge-state dependence points to the influence of the electronic energy loss.

III.2 - **EXAFS**

EXAFS signals and corresponding Fourier transforms at the Co and Cu K-edges are shown in Figure 4 and 5, for the as deposited and irradiated MLs (for the highest fluence and projectile charge-state). The EXAFS spectra present well-defined oscillations with the typical pattern of the fcc/hcp structure. No significant modification is observed after the irradiation for both edges. This is also clear from the Fourier transforms (r-space) that the contributions of next nearest neighbors are well defined in the as deposited and irradiated samples.

Excellent fits were obtained with the so-called R factor (a measure of the accuracy) being 0.007 for Cu and 0.03 for Co considering Cu and Co in a fcc structure. A typical fit result is shown in Fig. 6 for the Cu K-edge of the irradiated sample. The quantitative analysis (Table 2) suggests that the Co-Co and Cu-Cu distances for the first shell are around 2.51 Å with low disorder. The EXAFS results indicate that the atomic local order around the Co and Cu atoms is largely preserved in the MLs after the irradiation. However, any mixing resulting in exchanging Cu and Co cannot be observed, as the corresponding variations of the atomic distances (roughly 0.01 Å) cannot be resolved.

III.3 - **GMR**

Figure 7 displays the MR results for the as deposited and irradiated films. For the as deposited films (curve a), clear GMR with a relative resistivity enhancement of about 41% over the saturation value is observed. The maximum MR amplitude decreases with increasing ion fluence (curves b and d for the smallest projectile charge-state and curves c and e for the largest projectile charge-state). However, for the same fluence, the amplitudes are almost insensitive to the projectile charge state (see Table 1 and curves b and c or d and e).

III.4 - **Magnetization**

The normalized magnetization curves for the as deposited sample are shown in Fig. 8. For the as deposited film, the curve exhibits a small remanent magnetization (M_r) and a slow approach to saturation, indicating a significant interlayer antiferromagnetic coupling (see values in Table 1). With the increasing ion fluence, we note an increase of the direct ferromagnetic coupling, with the increase of the M_r and rapid approach to saturation, probably caused by the presence of the pinholes. The effect of the charge state is negligible, since the M_r value does not change significantly when the charge state changes from Au^{30+} to $Au^{46.3+}$ for both fluences, although some differences can be observed (see Table 1) for the smallest fluence.

IV - Discussion

The subtle modification in the microstructure induces distinct changes in the magnetization curves (increase of the M_r) and a strong decrease of the GMR effect with increasing fluence. The correlation between changes in the GMR and M_r suggests that the main effect responsible for the decrease of the GMR is caused by ferromagnetic pinhole creation.

In principle these pinholes could be the ion tracks themselves. In fact the energy transfer to electronic excitations is so huge that demagnetization inside of the ions track could be expected. Because of the metallic behavior of the samples, effects of Coulomb explosion [1-3] could be ruled out, considering the short live time of the positive spatial charge along the ion track. Instead, in theses systems one may expect a formation of hot electronic plasma around the ion track according to the electronic thermal spike model [4-9] . Since the electron temperature can be extremely high [45], some modification of the microstructure can take place through the electron-phonon coupling. Nevertheless, it depends on the electronic energy density delivered by the ion beam and the migration energy of the different atoms in the present magnetic MLs. Although the electronic stopping power of 593 MeV Au ions is very large, it is possible that it is not large enough to create a permanent ion track or to produce an interface mixing in the investigated ML system. There might be a strong recrystallization tendency and only some energy-loss fluctuations (discontinuous ion track) would lead to permanent changes. This could explain the subtle changes of the microstructure observed by XRD and EXAFS. However, the use of two different projectile charge states (the use of different electronic excitations) should have produced distinct discontinuous ion tracks, which would affect the GMR and the magnetization measurements. Nevertheless, as can be observed in Figure 7 and 8, both measurements do not depend on the projectile charge.

Another issue to be observed is the effect of the nuclear stopping power. Although the energy given to set up atomic motion in cascades is about 300 times smaller than the energy delivered to electronic excitations, its absolute value is not negligible. In fact it is smaller than the ones used in low-energy experiments (a factor of 2 for 40 keV Ne experiments [46] and a factor of 6 for 200 keV Ar experiments [47]). However, the product of specific nuclear energy loss and fluence for the onset of magnetic effects in these low-energy experiments is about the same as in current experiments. Moreover, the nuclear energy loss at the present energy range is weakly sensitive to the projectile charge-state since the target is neutral, limiting the range of the potential. In that way, the present results, which are in fact very similar to the findings observed at lower irradiation energies such as with 200 keV Ar-ions in Fe/Cr MLs [47], indicate that the nuclear stopping power is probably responsible for a pinhole creation.

Concluding Remarks

We have observed changes in the magneto resistance and magnetization with swift Au irradiations, which are probably related to ferromagnetic pinholes. However, they are not produced directly by electronic spikes since these changes are weakly sensitive on the projectile-charge state, which in turn causes a large variation of the electronic energy deposited in the present Co/NiFe/Co/Cu ML system.

Instead, the nuclear energy transfer to atomic cascades should be responsible for the observed reduction of the GMR and increase of the M_r without affecting their microstructure. Nevertheless, some interplay between electronic and nuclear energy loss processes cannot be completely ruled out because the measurements of the reflectivity indicate some significant differences (long range order, possibly interface roughness), which depend on the charge-state of the projectile. The same holds true for the remanent magnetization measurements, where the largest projectile charge-state induced a somewhat larger M_r for the smallest fluence. The local atomic order might be preserved as indicated by EXAFS, but the expected effects are most likely below the EXAFS accuracy limit.

Acknowledgements

The authors are indebted with the Brazilian agencies CAPES (PROBRAL 166/04), CNPq and FAPERGS for the partial support to this work. The use of the irradiation and beam-wobbling facility of S. Klaumünzer for the irradiations is gratefully acknowledged. We would like also to thank him for very fruitful and stimulating discussions.

The authors also thank G.I. Weizenmann and D.U. Pauly for assistance with magnetization and magnetoresistance measurements. We are indebted to the staff of LNLS for operating the storage ring and the assistance during the experiments at the XAFS1 beam line. The beam time was supported by LNLS under the project XAFS1 2304

References

[1] R.E. Johnson and W.L. Brown, Nucl. Instr. and Meth. **B198**, 103-118 (1982).

[2] A. Akkermann , J. Levinson, D. Ilberg and Y. Lifshitz , Ionization of Solids by Heavy Particles ed. by R. Baragiola, NATO Advanced Study Institutes Series 306, Plenum Press, New York and London, 431-438 (1992).

[3] D. Leseur and A. Dunlop, Rad. Eff. and Def. Solids **126**, 163-172 (1993).

[4] F. Desauer, Z. Phys. **12**, 38 (1923).

[5] I.M. Lifshitz, M.I. Kaganov and L.V. Tanatarov, J. Nucl. Energy **A12**, 69 (1960).

[6] R.H. Ritchie and C. Claussen, Nucl. Instr. and Meth. B198, 133 (1982).

[7] Z.G. Wang, C. Dufour, E. Paumier and M. Toulemonde, J. Phys.: Condens. Matter **6**, 6733 (1994).

[8] G. Szenes, Nucl. Instr. Meth. **B116**, 141 (1996).

[9] A.E. Volkov and V.A. Borodin, Nucl. Instr. Meth. **B107**, 172 (1996).

[10] R.L. Fleischer, P.B. Price, and R.M. Walker, "Nuclear Tracks in Solids" (University of California Press, Berkely California, 1975).

[11] R. Spohr; "Ion tracks and microtechnology" (F.Vieweg und Sohn Verlagsgesellschaft, Braunschweig 1990).

[12] M.N. Baibich, J.M. Broto, A. Fert, F. Nguyen Van Dau, F. Petroff, P. Etienne, G. Creuzet, A. Friederich and J. Chazelas, Phys. Rev. Lett. **61** , 2472 (1988).

[13] C. Tsang, R. Fontana, T. Lin, D. Heim, V. Speriosu, B. Gurney, and M. William, IEEE Trans. Magn. **30**, 3801 (1994).

[14] R. Gupta, K. -H. Han, K.P. Lieb, G.A. Mueller, P. Schaaf and K. Zhang, J. Appl. Phys., **97**, 073911 (2005).

[15] K. Zhang, R. Gupta, G.A. Mueller, P. Schaaf and K.P. Lieb, App. Phys. Lett. **84**, 3915 (2004).

[16] R. Gupta, G.A. Mueller, P. Schaaf, K. Zhang, K.P. Lieb, Nuclear Instr. and Methods in Phys, Research **B 216** , 350 (2004).

[17] K. Zhang, K.P. Lieb, M. Marszalek, V. Milinovic, V. Tokman, Thin Solid Films **515**, 700 (2006).

[18] T. Mewes, R. Lopusnik, J. Fassbender, B. Hillenbrands, M. Jung, D. Engel, A. Ehresmann, H. Schmoranzer, Appl. Phys. Lett., **76**, 1057 (2000).

[19] C. Chappert, H. Bernas, J. Ferré, V. Kottler, J.P. Jamet, Y. Chen, E. Cambril, T. Devolder, F. Rousseaux, V. Mathet, H. Launois, Science **280**, 1919 (1998).

[20] S.O. Demokritov, C. Bayer, S. Poppe, M. Rickart, J. Fassbender, B. Hillebrands, D.I. Kholin, N.M..Kreines, O.M. Leidke, Phys. Rev. Lett. **90**, 097201-1(2003).

[21] H. Bernas, J.-Ph. Attané, K.H. Heinig, D. Ravelosona, A. Marthy, P. Auric, C. Chappert, Y. Samson, Phys. Rev. Lett. **91**, 077203-1 (2003).

[22] V. Milinovic, K.P. Lieb, P.K. Sahoo, P. Schaaf, K. Zhang, S. Klaumuenzer, M. Weisheit, Appl. Surf. Science, **252**, 5339 (2006).

[23] K. Zhang, K.P. Lieb, V. Milinovic, P.K. Sahoo, J. of Appl. Phys. **100**, 053501 (2006).

[24] M. Cai, T. Veres, F. Schiettekatte, S. Roordam R.W. Cochrane,. J. Appl. Phys. **95**, 2006 (2004).

[25] T, Veres, P.Desjardins, R.W. Cochrane, M. Cai, M. Rouabhi, L. Cheng, R. Abdouche, M. Sutton, Thin Solid Films **382**, 164 (2001).

[26] T. Veres, M. Cai, R.W. Cochrane, S. Roorda, J. Appl. Phys. **87**, 8504 (2000).

[27] E. Kerr, S. van Dijken, R.M. Langford, J.M.D. Coey, Journal of Magnetism and Magnetic Materials **290**, 124 (2005).

[28] A. Paul, A. Gupta, S.M. Chaudhari, D.M. Phase, Vacuum **60**, 401 (2001).

[29] R. Gupta, A. Gupta, D.K. Avasthi, G. Principi and G. Tosello, Nuclear Instr. and Methods in Phys, Research **B 156**, 153 (1999).

[30] A. Dogra, R. Kumar, S.A. Kahn, V.V. Siva Kumar, N. Kumar, M. Singh, Nuclear Instr. and Methods in Phys, Research **B 225** , 283 (2004).

[31] L. C. C. M. Nagamine, A. Biondo, L. G. Pereira, A. F. Souza, A. Mello, J. E. Schmidt, M. B. Fontes, E. Baggio Saitovitch, Journal of Magnetism and Magnetic Materials **242-245**, 541 (2002).

[32] L. C. C. M. Nagamine, A. Biondo, L. G. Pereira, A. Mello, J. E. Schmidt, T. W. Chimendes, J. B. M. Cunha, and E. B. Saitovitch, J. Appl. Phys. **94**, 5881 (2003).

[32a] F. Ono, Y. Hamatani, Y. Mukumoto, S. Komatsu, N. Ishikawa, Y. Chimi, A. Iwase, T. Kambara, C. Mueller, R. Neumann, Nucl. Instr. and Methods B **206**, 295-298 (2003).

[32b] F. Ono, S. Komatsu, Y. Chimi, N. Ishikawa, A. Iwase, T. Kambara, Nucl. Instr. and Methods B **230**, 279-283 (2005).

[32c] Y. Matsushima, N.Q. Sun, H. Kanamitsu, M. Matsushita, A. Iwase, Y. Chimi, N. Ishikawa, T. Kambara, F. Ono, Journal of Magnetism and Magnetic Materials **298**, 14-18 (2006).

[33] J. Fassbender, J. von Borany, A. Muecklich, K. Potzger, W. Moeller, J. McCord, L. Schultz, R. Mattheis, Physical Review B **73**, 184410 (2006).

[34] S. I. Woods, S. Ingvarsson, J.R. Kirtley, H.F. Hamann, R.H. Koch, App. Phys. Lett. **81**, 1267 (2002).

[34a] A. Dunlop, D. Lesueur, P. Legrand and H. Dammak, Nucl. Instr. and Methods B **90**, 330-338 (1994).

[34b] H. Dammak, A. Dunlop, D. Lesueur, Nucl. Instr. and Methods B 107, 204-211 (1996).

[35] V.S.Nikolaev and I.S.Dmitriev, Phys. Lett. **28A**, 277 (1968).

[36] G. Schiwietz and P.L. Grande, Nucl. Instr. and Methods B **175**, 125-131 (2001).

[37] G. Schiwietz , K. Czerski, M. Roth. F. Staufenbiel, P.L. Grande , Nucl. Instr. and Methods B **225**, 4-26 (2004).

[38] J.F. Ziegler, Computer code SRIM code, http://www.SRIM.org.

[39] H. C. N. Tolentino, A.Y. Ramos, M. C.M. Alves, R. A. Barrea, E. Tamura, J. C. Cezar, N. Watanabe, J. Synchrotron Rad. **8**, 1040-1046, (2001).

[40] M Newville, J. Synchrotron Rad. **8**, 322-324 (2001).

[41] J.J. Rehr & R.C. Albers, Rev. Mod. Phys. **72**, 621-654 (2000)

[42] B. Ravel, J. Synchrotron Rad. **8**, 314-316 (2001)

[43] P. F Fewster, Rep. Prog. Phys. **59**, 1339 (1996).

[44] E. E. Fullerton, D. M. Kelly, J. Guimpel, I. K. Schuller, Y. Bruynseraede, Phys. Rev. Lett. **68**, 859 (1992).

[44a] S. Klaumuenzer, private communication; S. Klaumuenzer, W. Assmann and J. Gerlach , HMI - B602 annual Report 2004.

[44b] A. Hedler, PhD. thesis, Univ. Jena, Germany (2006); A.Hedler, S. Klaumuenzer und W. Wesch, submitted to Phys. Rev. B (2006).

[45] G. Schiwietz, G. Xiao, P.L. Grande, E. Luderer, E. Pazirandeh, U. Stettner, Europhysics Letters **47**, 384 (1999).

[46] R. Gupta, K.H. Han, K.P. Lieb, G.A. Mueller, P. Schaaf and K. Zhang, J. Appl. Phys**.** **97**, 73911 (2005).

[47] M. Kopcewicz, F.Stobiecki, J. Jagielski, B. Symanski, M. Schmidt, J. Dubowik, J. Kalinowska, J. Appl. Phys. 93**, 5514 (2003).**

Figure Captions

Fig. 1- Experimental and fitted mean exit charge-state for normal incident 593 MeV $^{197}Au^{30+}$ ions behind amorphous carbon foils of different projected mass densities (the actual energy delivered by the accelerator was 593 MeV). The fits account for the charge-state variation due to the ion energy-loss in the foils.

Fig. 2- Large-angle x-ray diffraction spectra for as deposited and after irradiation at 3×10^{13} Au^{+30}/ cm^2. The curves have been displaced by 3000 counts/s for clarity.

Fig. 3- Small-angle reflectivity spectra (a) as deposited, (b) after irradiation with 3×10^{13} Au^{+30}/ cm^2, (c) with 3×10^{13} $Au^{+46.3}$/ cm^2, (d) with 6×10^{13} Au^{+30}/ cm^2, (e) with 6×10^{13} $Au^{+46.3}$/ cm^2. The curves have been displaced vertically for clarity.

Fig. 4- EXAFS signals at the Co and Cu *K* edges for as deposited and irradiated with highest fluence and projectile charge-state multilayers.

Fig. 5- Radial distribution function produced by forward Fourier transforms of the EXAFS spectra over the k range 2.2-11.8 $Å^{-1}$.

Fig. 6- Fitting of the Fourier transformed modulus and real part for the Cu K-edge of the irradiated sample.

Fig. 7- Magnetoresistance as function of the applied field of [Co 5Å/NiFe 16 Å/ Co 5Å/ Cu 9Å]20, where the asterisks represent the data for as deposited ML, circles after irradiation with 3×10^{13} Au/cm^2 and triangles with 6×10^{13} Au/cm^2. Open symbols represent Au^{30+} and closed symbols represent $Au^{46.3+}$ion charge state. The labels are the same as in Fig. 3.

Fig. 8– Normalized hysteresis curves for [Co 5Å/NiFe 16 Å/ Co 5Å/ Cu 9Å]20, where the asterisks represent the data for as deposited ML, circles after irradiation with 3×10^{13} Au/cm^2 and triangles with 6×10^{13} Au/cm^2. Open symbols represent Au^{30+} and closed symbols represent $Au^{46.3+}$ion charge state. The labels are the same as in Fig. 3.

Tables

Table 1 – Values of the Bragg peak amplitude, remanent magnetization and magnetoresistance amplitudes, extracted from Fig. 3, Fig. 8 and Fig. 7, respectively.

Sample	*Amplitude (counts/s)*	$M_{\mathbf{r}}$	**MR (%)**
a) **as deposited**	114	0.27±0.01	41
b) 3×10^{13} Au^{30+}/cm^2	80	0.51±0.01	28
c) 3×10^{13} $Au^{46.3+}$/cm^2	26	0.56±0.01	27
d) 6×10^{13} Au^{30+}/cm^2	53	0.68±0.01	17
e) 6×10^{13} $Au^{46.3+}$/cm^2	8	0.69±0.01	18

Table 2 – Structural parameters obtained from the fits. ΔR is the distance variation with respect to the bulk metal, σ^2 is the Debye-Waller factor, S_0^2 is the passive electron reduction factor and E_0 is the energy shift.

Sample	**ΔR (Å)**	**σ^2 (Å^2)**	**S_0^2**	**E_0 (eV)**
		Co K- edge		
as deposited	- 0.0098	0.0079 ± 0.0016	0.70 ± 0.09	7.9 ± 1.0
irradiated	- 0.0098	0.0078 ± 0.0016	0.70 ± 0.06	7.9 ± 1.0
		Cu K- edge		
as deposited	- 0.044	0.0131 ± 0.0026	0.79 ± 0.09	3.9 ± 1.0
irradiated	- 0.032	0.0136 ± 0.0027	0.79 ± 0.01	3.9 ± 0.3

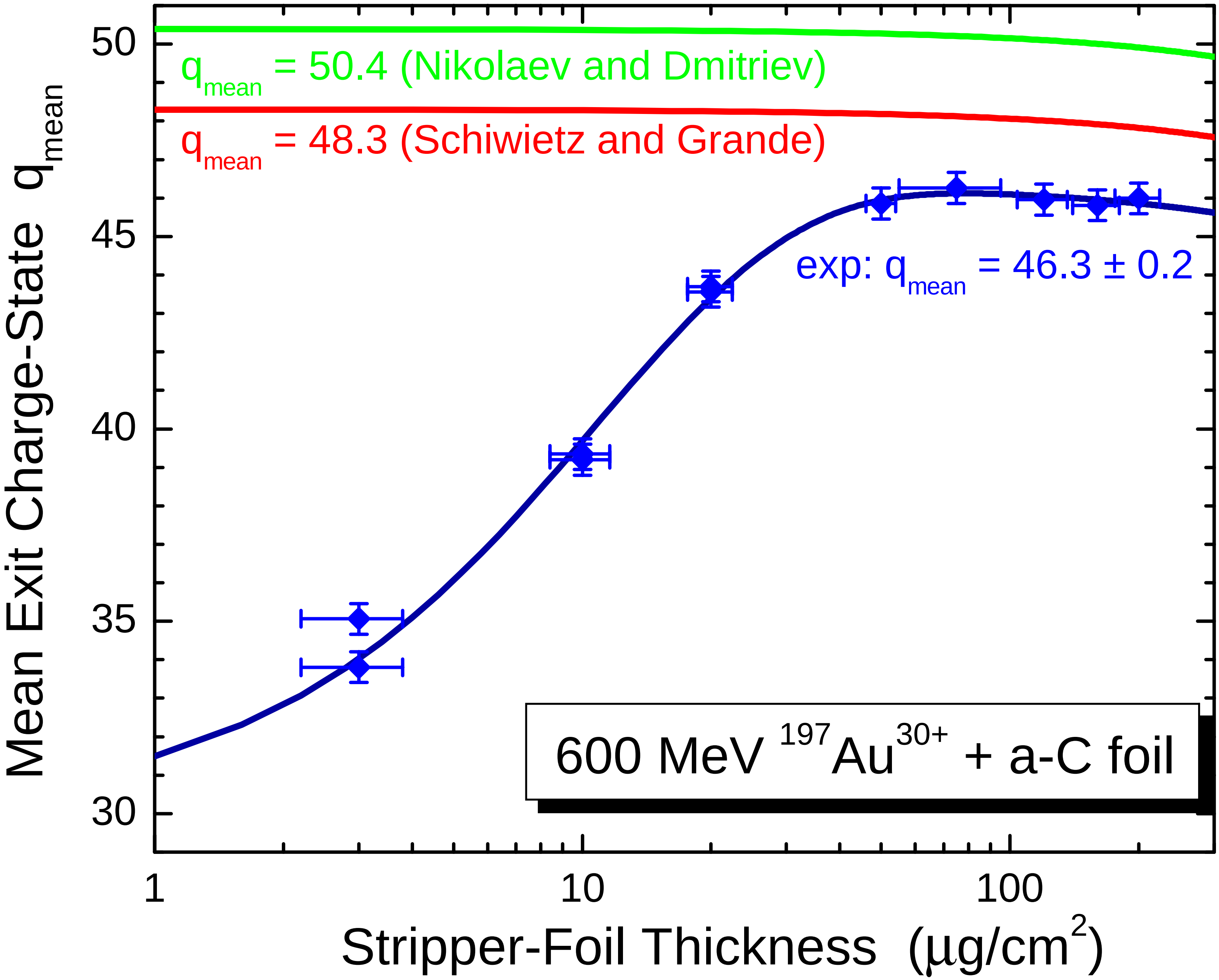

Mean Exit Charge-State q_{mean}
Stripper-Foil Thickness (μg/cm^2)
q_{mean} = 50.4 (Nikolaev and Dmitriev)
q_{mean} = 48.3 (Schiwietz and Grande)
exp: q_{mean} = 46.3 ± 0.2
600 MeV $^{197}Au^{30+}$ + a-C foil
50
45
40
35
30
1
10
100

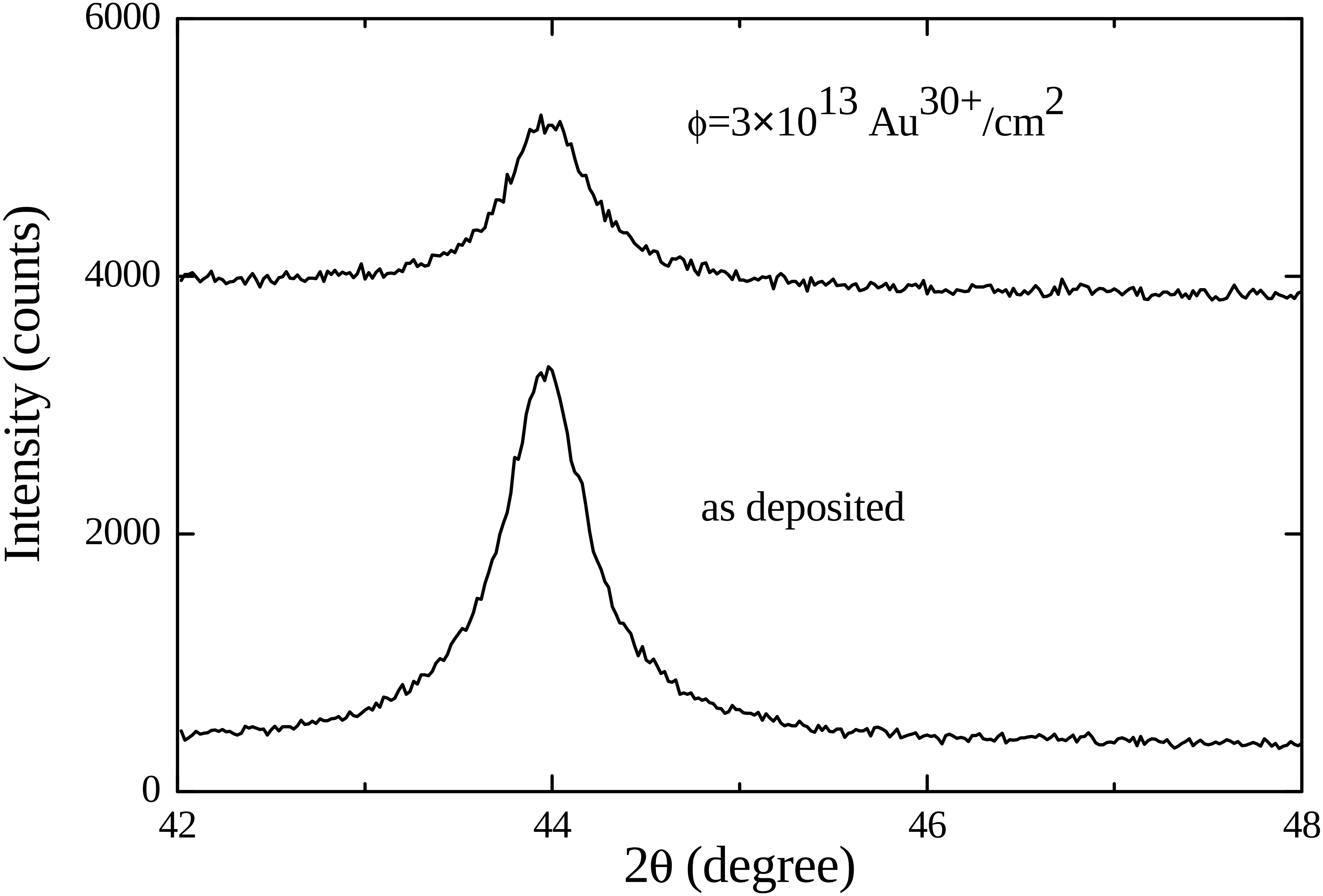

6000
4000
2000
0
42
44
46
48
Intensity (counts)
2θ (degree)
φ=3×10^13 Au^30+/cm^2
as deposited

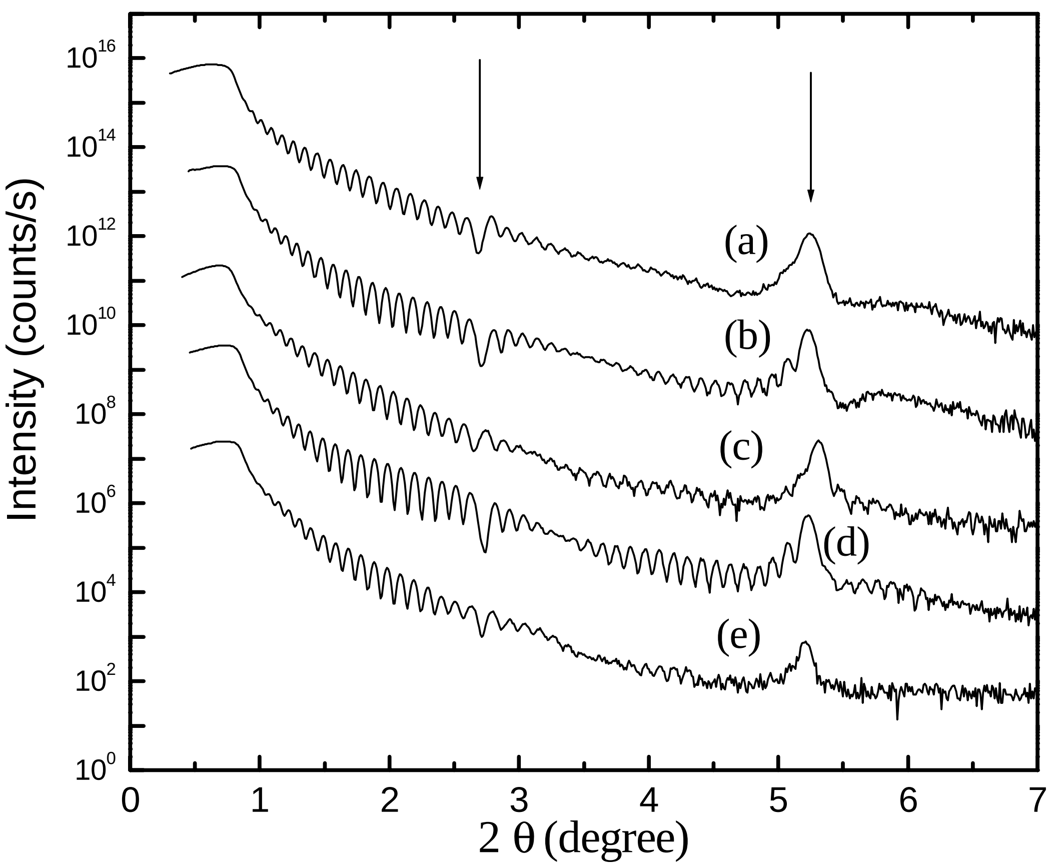

Intensity (counts/s)
10^16
10^14
10^12
10^10
10^8
10^6
10^4
10^2
10^0
0
1
2
3
4
5
6
7
2 θ (degree)
(a)
(b)
(c)
(d)
(e)

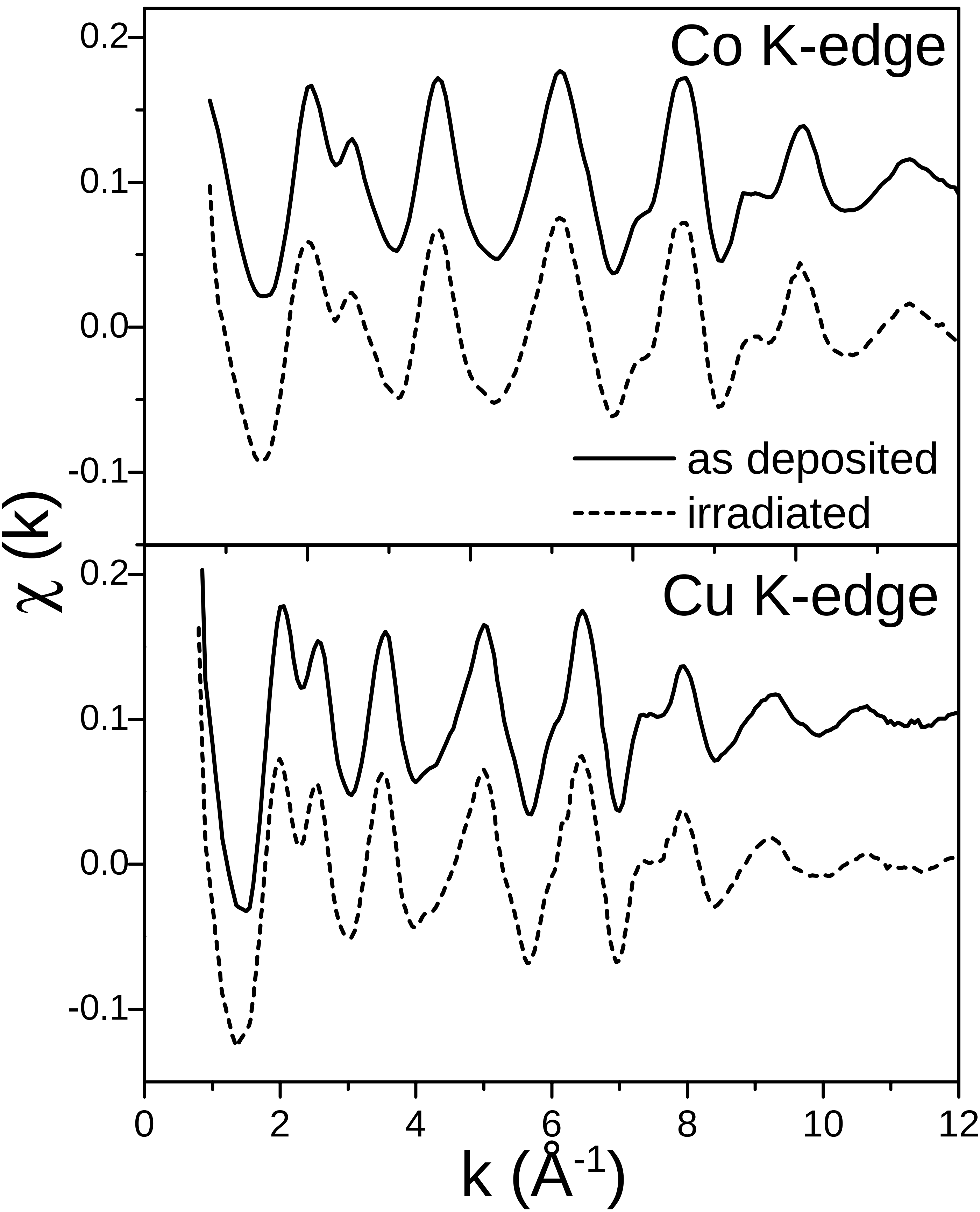
Co K-edge
as deposited
irradiated
Cu K-edge
χ (k)
k (Å-1)
0.2
0.1
0.0
-0.1
0
2
4
6
8
10
12

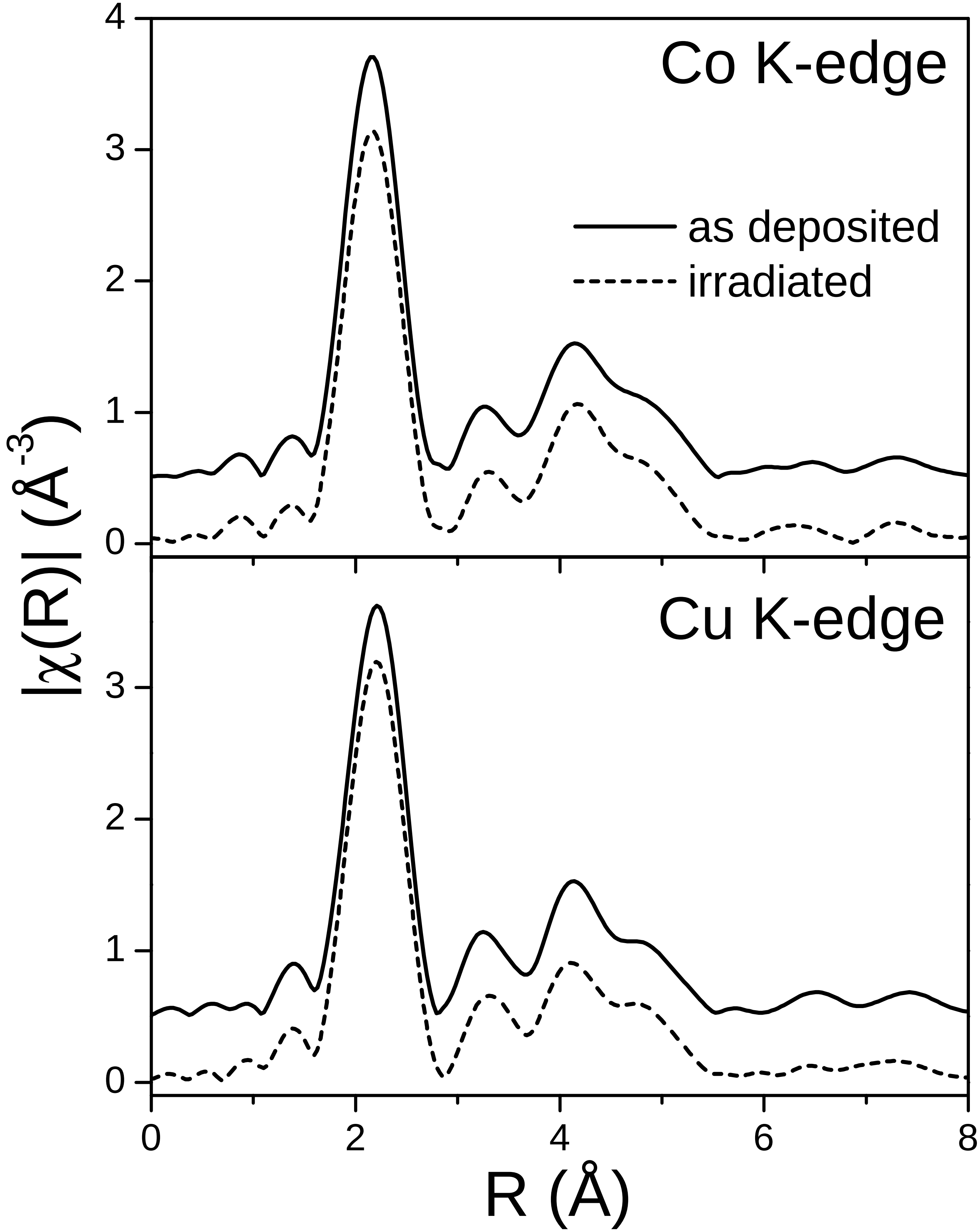

Co K-edge
as deposited
irradiated
Cu K-edge
|χ(R)| (Å^{-3})
R (Å)
0
1
2
3
4
0
2
4
6
8

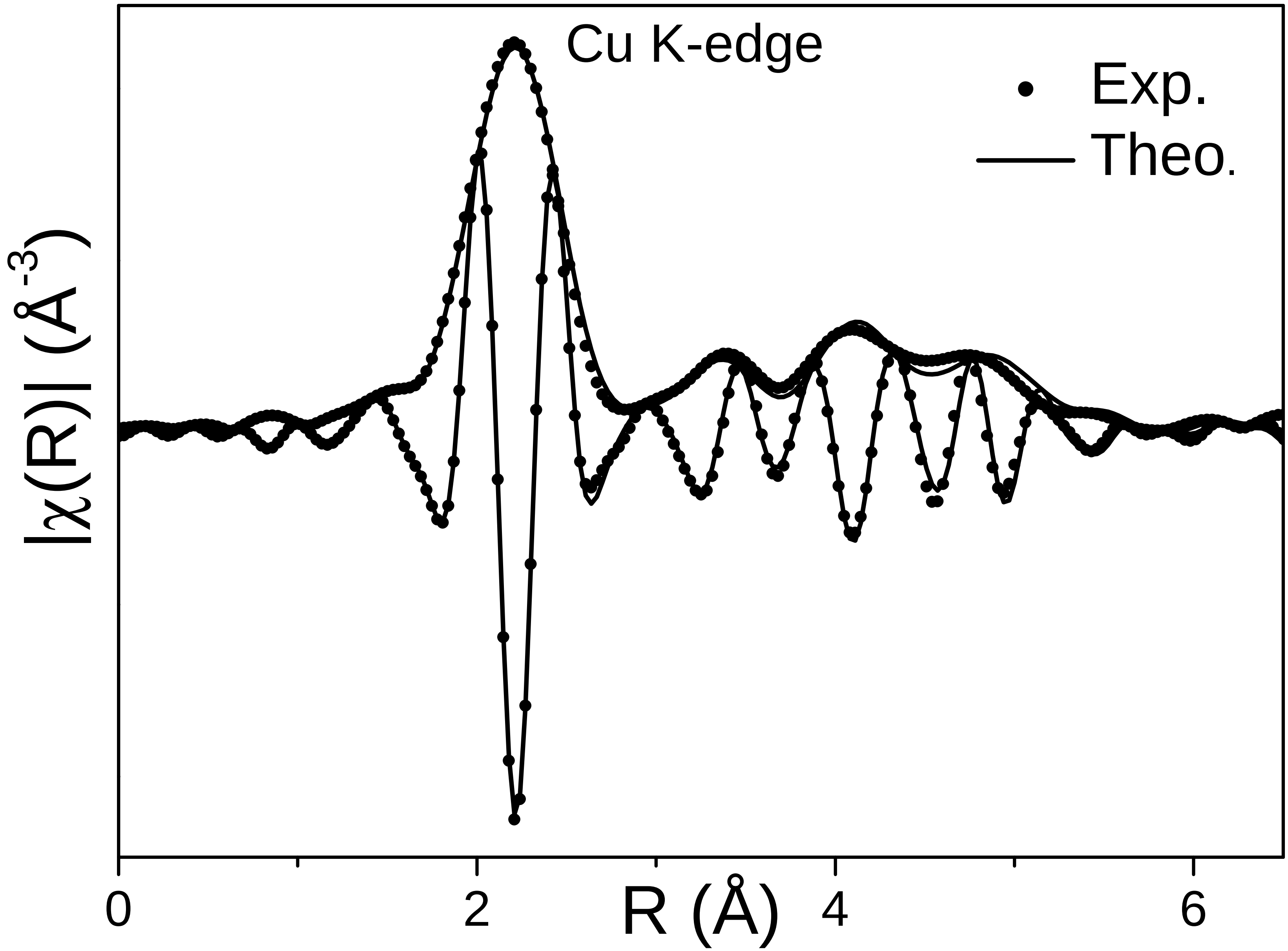
Cu K-edge
Exp.
Theo.
|χ(R)| (Å^{-3})
R (Å)
0
2
4
6

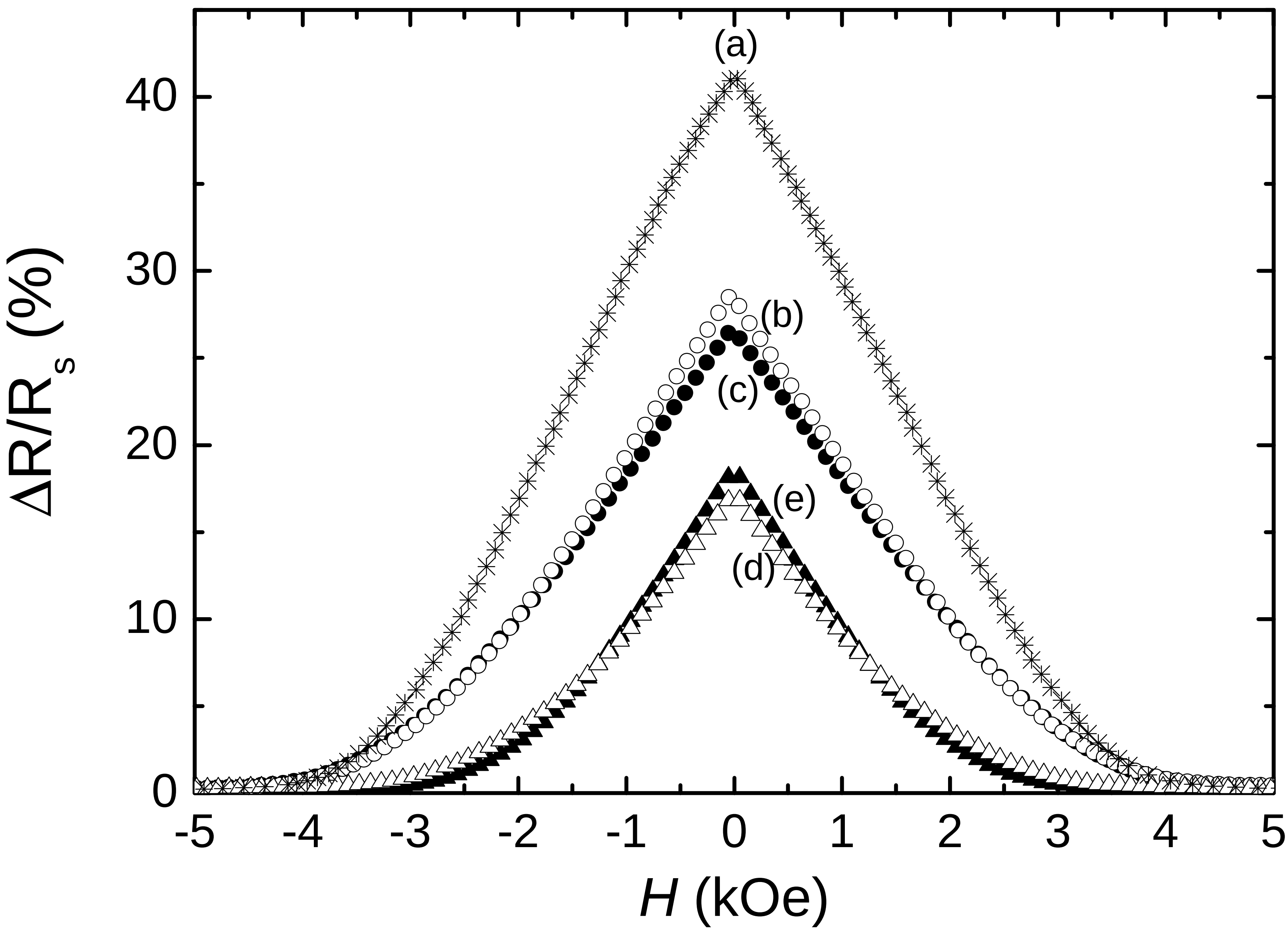

(a)
(b)
(c)
(d)
(e)
0
10
20
30
40
ΔR/R_s (%)
-5
-4
-3
-2
-1
0
1
2
3
4
5
H (kOe)

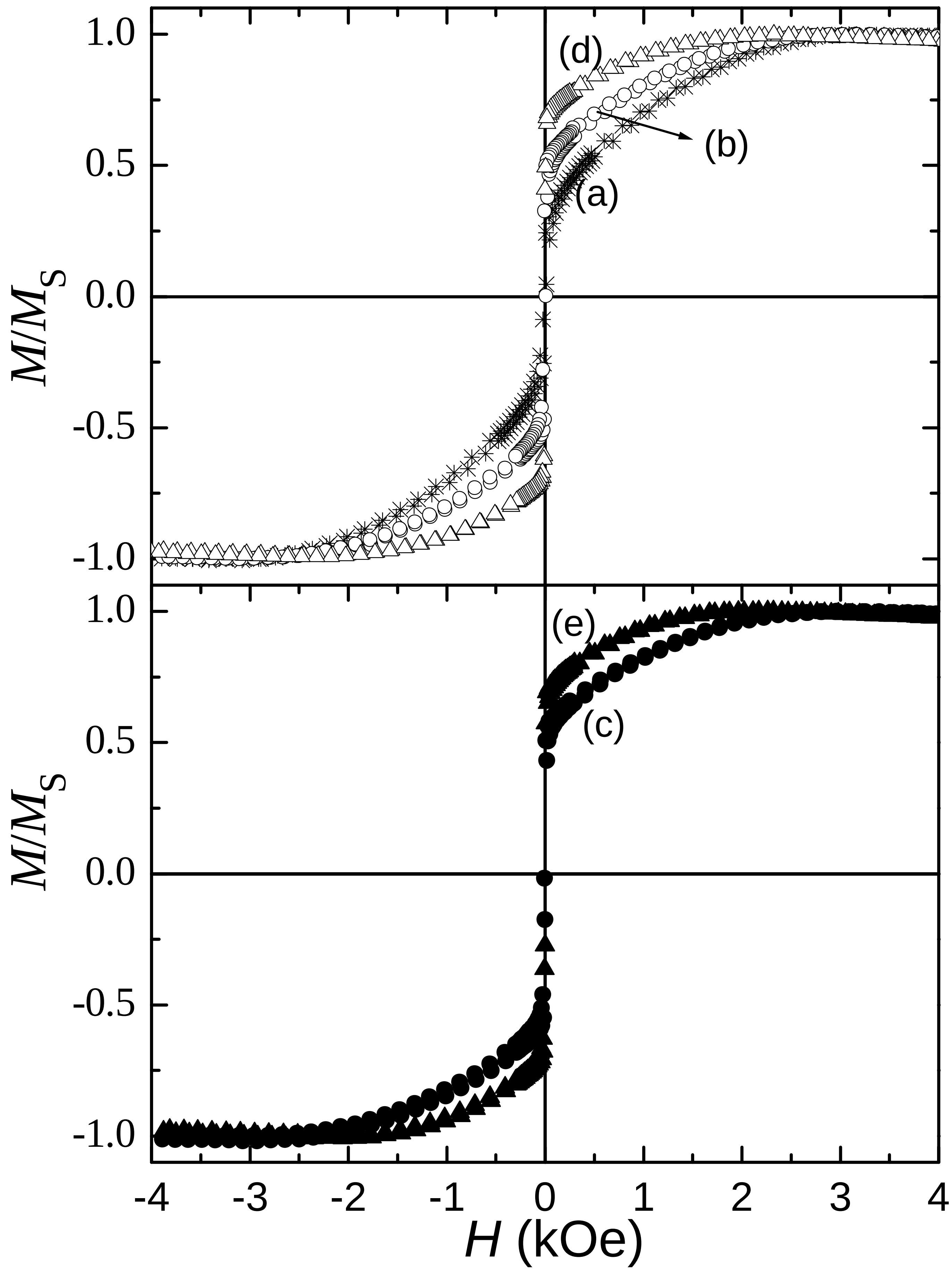

1.0
0.5
0.0
-0.5
-1.0
M/M_S
(d)
(b)
(a)
(e)
(c)
-4
-3
-2
-1
0
1
2
3
4
H (kOe)